IEEE Access
Multidisciplinary | Rapid Review | Open Access Journal

Received June 20, 2020, accepted July 5, 2020, date of publication July 14, 2020, date of current version July 27, 2020.

Digital Object Identifier 10.1109/ACCESS.2020.3009266

ECG Signal Reconstruction via Doppler Sensor by Hybrid Deep Learning Model With CNN and LSTM

KOHEI YAMAMOTO[1], (Graduate Student Member, IEEE), RYOSUKE HIROMATSU[1], (Student Member, IEEE), AND TOMOAKI OHTSUKI[2], (Senior Member, IEEE)

[1]Graduate School of Science and Technology, Keio University, Kanagawa 223-8522, Japan
[2]Department of Information and Computer Science, Keio University, Kanagawa 223-8522, Japan

Corresponding author: Kohei Yamamoto (yamamoto@ohtsuki.ics.keio.ac.jp)

ABSTRACT An Electrocardiogram (ECG) is a typical method used to detect heartbeat, and an ECG signal analysis enables the detection of some heart diseases. However, the ECG-based heartbeat detection requires device attachment, which is not preferred for daily use. A Doppler sensor could be a device used to enable the non-contact heartbeat detection. In this paper, we propose a Doppler sensor-based ECG signal reconstruction method by a hybrid deep learning model with Convolutional Neural Network (CNN) and Long Short-Term Memory (LSTM). An ECG signal can be reconstructed by relating features of a heartbeat signal obtained by a Doppler sensor to those of the ECG signal. Thus, we construct the deep learning model that extracts the spatial and temporal features from the heartbeat signal by CNN and LSTM. Based on the extracted features, the ECG signal is reconstructed. We conducted experiments to observe heartbeat against 9 healthy subjects without heart disease. The experimental results showed that our method performed ECG signal reconstruction with a correlation coefficient of 0.86 between the reconstructed and actual ECG signals, even without attaching devices. The results indicate that it is possible to remotely reconstruct an ECG signal from a heartbeat signal via a Doppler sensor.

INDEX TERMS Heartbeat, microwaves, Doppler sensor, ECG, deep learning.

I. INTRODUCTION

Heartbeat is one of the most important biological signals to grasp our health condition. Thus, the technique of the heartbeat detection has been required in various fields, e.g., the medical field [1], [2], the health care field [3], [4], and the smart home field [5], [6]. Electrocardiogram (ECG) is a typical heartbeat detection method. Fig 1 shows an example of an ECG signal. Once the atrial activation starts, a P-wave appears, and subsequently, an R-peak appears due to the ventricular activation. As the ventricle gets relaxed, a T-wave finally appears. By analyzing the timing when the P-wave, the T-wave, and the R-peak appear, various heart diseases can be detected [7]–[9]. However, to detect heartbeat with an ECG, it is necessary to attach electrodes to a body, which is not suitable for daily heartbeat detection.

As one of the non-contact heartbeat detection methods, a Doppler sensor-based method has been studied intensively [10]–[23]. A Doppler sensor is a device that transmits microwaves toward a target and receives the microwaves reflected by the target. At the same time of the reflection, the microwaves are Doppler-shifted. Thus, it is possible to measure the velocity and direction of the target's motion by analyzing the received signal. Based on this principle, the use of a Doppler sensor has been investigated in various fields such as heartbeat detection [10]–[23], respiration detection [24]–[26], and activity recognition [27]–[29]. However, the Signal-to-Noise Ratio (SNR) of heartbeat components is low, compared to those of respiration and slight body movements. Hence, to accurately detect heartbeat, various Doppler sensor-based heartbeat detection methods have been proposed [10]–[23]. These conventional methods aim to estimate the beat-to-beat interval (BBI) and the heart rate (HR) and have been experimentally shown to achieve a high heartbeat detection accuracy. However, none of the conventional methods have detected the P-wave, the T-wave, and the R-peak, though various heart diseases can be identified by analyzing the timings when such features appear. As previously mentioned, the SNR of the heartbeat components could be lower due to respiration and slight body movements. Thus,

The associate editor coordinating the review of this manuscript and approving it for publication was Siddhartha Bhattacharyya.

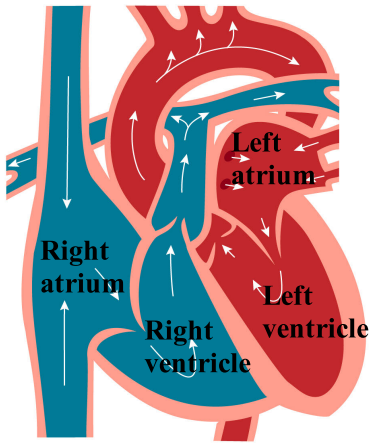

(a) An illustration of a heart .

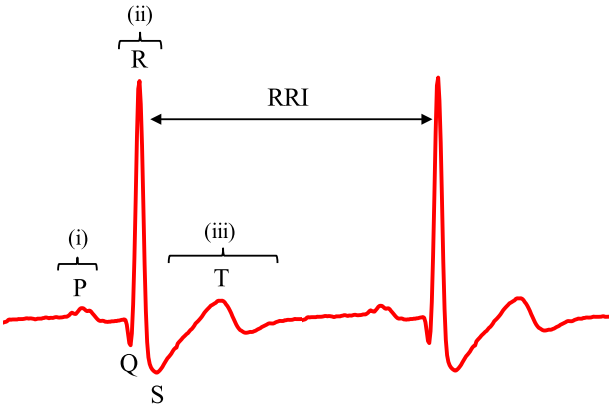

(b) An ECG signal.

FIGURE 1. (a) An illustration of a heart and (b) an ECG signal. (i) A P-wave appears due to the atrial activation, (ii) an R-peak does due to the ventricular activation, and (iii) a T-wave does due to the ventricular relaxation.

detecting the P-wave, the T-wave, and the R-peak is more difficult than detecting only heartbeat.

In this paper, to detect the P-wave, the T-wave, and the R-peak via a Doppler sensor, we propose an ECG signal reconstruction method by a hybrid deep learning model with Convolutional Neural Network (CNN) and Long Short-Term Memory (LSTM). In our method, a deep learning technique is used to solve a prediction problem, that is obtaining the ECG signal from the heartbeat signal obtained by a Doppler sensor. For the automatic feature extraction to reconstruct the ECG signal, the hybrid model with CNN and LSTM is proposed. Specifically, the heartbeat signal by a Doppler sensor can be deformed due to noise. This means that there exist numerous types of heartbeat signal waveforms. Therefore, we use deep learning techniques to automatically extract deep features that are useful for the ECG signal reconstruction, even from numerous types of the heartbeat signal waveforms. To transform the heartbeat signal to the ECG signal, temporal features of the heartbeat signal are very important. Hence, we use LSTM to extract the temporal features, e.g., the P-wave, the T-wave, and the R-peak appear successively. LSTM is

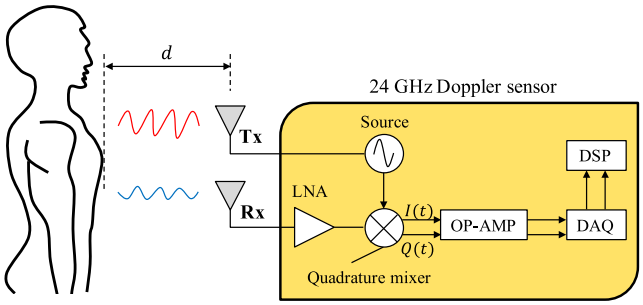

FIGURE 2. The system model of heartbeat detection with a Doppler sensor.

a deep learning technique that is useful to extract features of time sequence data [30], and it has been successfully applied to signal classification [31], [32] and prediction [33]. However, as aforementioned, a heartbeat signal is likely to be deformed due to noise. To make the model robust to this type of deformation, we first extract spatial features by CNN [34] that has been successful in the fields of image recognition [35], [36] and the signal classification [37]. After the spatial feature extraction, we extract temporal features by applying LSTM to the output of the CNN. An ECG signal is the final output based on the features extracted by the CNN and LSTM. Although the use of only CNN or LSTM might also enable the transformation of the heartbeat signal to the ECG signal, the use of both CNN and LSTM makes the model robust against the diversity of the heartbeat signal.

The novelty and contribution of this paper are as follows.

- Although ECG signal reconstruction has been conventionally realized by attaching devices, these methods can make a subject uncomfortable in long-term monitoring in daily life. In this paper, we propose a non-contact ECG signal reconstruction via a Doppler sensor.
- We discuss the characteristics of a heartbeat signal by a Doppler sensor. Based on that, we combine the benefits of CNN and LSTM, and construct a hybrid deep learning model that transforms the heartbeat signal to an ECG signal.
- We show that the proposed method has a good ability to reconstruct an ECG signal. Additionally, we compare our ECG signal reconstruction with the ECG signal reconstruction by attaching devices, and we show the feasibility of the non-contact ECG signal reconstruction via a Doppler sensor.

The rest of this paper is organized as follows. In Sections II and III, we explain the principle of a Doppler sensor and related works, respectively. We then propose an ECG signal reconstruction method in Section IV, and evaluate the performance of our method in Section V. Finally, we conclude this paper in Section VI.

II. SYSTEM MODEL OF HEARTBEAT DETECTION WITH DOPPLER SENSOR

In this section, we describe the system model of heartbeat detection with a Doppler sensor. The fundamental principle of

a Doppler sensor is to measure the frequency change caused by the Doppler effect. Fig. 2 shows the system model of heartbeat detection with a Doppler sensor. Microwaves are transmitted from a Doppler sensor toward a subject' chest. When the chest reflects the microwaves, the phase of the microwaves is Doppler-shifted by the chest's displacements due to the subject's heartbeat. The Doppler-shift due to the heartbeat, $f_{Doppler}$, can be expressed as follows.

$$f_{Doppler} = \mp\frac{4\pi vt}{\lambda} \times \frac{1}{2\pi t} = \mp\frac{2v}{\lambda}, \tag{1}$$

where v denotes the speed of the chest displacement. When the chest moves away from the Doppler sensor, the minus symbol can be adapted, and vice versa. The Doppler sensor then receives the reflected microwaves. The received signal is passed through the low noise amplifier (LNA) and down-converted into the baseband signal $B(t)$. When the chest is a distance d from the Doppler sensor, the baseband signal $B(t)$ can be expressed by the wavelength of the carrier λ as eq. (2).

$$B(t) = \cos\left(\theta + \frac{4\pi x_h(t)}{\lambda} + \Delta\Phi(t)\right), \tag{2}$$

where θ is the constant phase that is dependent on d and the carrier frequency f. Additionally, $x_h(t)$ is the chest displacement caused by the heartbeat, and $\Delta\Phi(t)$ is the total residual phase noise through the circuit and the transmission path. Subsequently, $B(t)$ is demodulated by a quadrature mixer, and two signals, namely, $I(t)$ and $Q(t)$, which are called in-phase and quadrature signals, respectively, are obtained as follows.

$$I(t) = \cos\left(\theta + \frac{\pi}{4} + \frac{4\pi x_h(t)}{\lambda} + \Delta\Phi(t)\right), \tag{3}$$

$$Q(t) = \cos\left(\theta - \frac{\pi}{4} + \frac{4\pi x_h(t)}{\lambda} + \Delta\Phi(t)\right). \tag{4}$$

$I(t)$ and $Q(t)$ are then amplified by the operational amplifier (OP-AMP). After the data acquisition (DAQ), the heartbeat can be detected by applying signal processing to the digitized $I(t)$ and $Q(t)$ in the digital signal processing (DSP).

III. RELATED WORKS

In this section, we describe other existing researches related to this work. An ECG is a heartbeat detection method that has been widely used in the medical field. Features of an ECG signal, e.g., the P-wave, the T-wave, and the R-peak, reflect the heart activity, and thus it is possible to detect some heart diseases by analyzing an ECG signal. Photoplethysmography (PPG) is a device that can emit light on a skin and observe the intensity variation of the reflected light. Since such intensity variation reflects the heart's activity, heartbeat can be detected by analyzing a PPG signal. Some researches have proposed accurate heartbeat detection methods with a PPG sensor mounted in wrist-type devices such as smartwatches [38]–[40]. Additionally, Q. Zhu *et al.* have proposed an ECG signal reconstruction method via a PPG signal [41]. In this method, an ECG signal is reconstructed by mapping the Discrete Cosine Transform (DCT) coefficients of the heartbeat signal by PPG to those of the ECG signal. In addition to ECG and PPG, Seismocardiogram (SCG) has also been used for heartbeat detection [42]–[44]. SCG can detect heartbeat by measuring the chest vibration and can capture the aortic valve opening and closing behavior, as well as the mitral valve opening and closing behavior. J. Park *et al.* have proposed an ECG signal reconstruction method via an SCG signal by using a deep learning model with bidirectional-LSTM [45]. Although these ECG signal reconstruction methods have been experimentally shown to be able to reconstruct the ECG signal, PPG and SCG essentially require the device attachment.

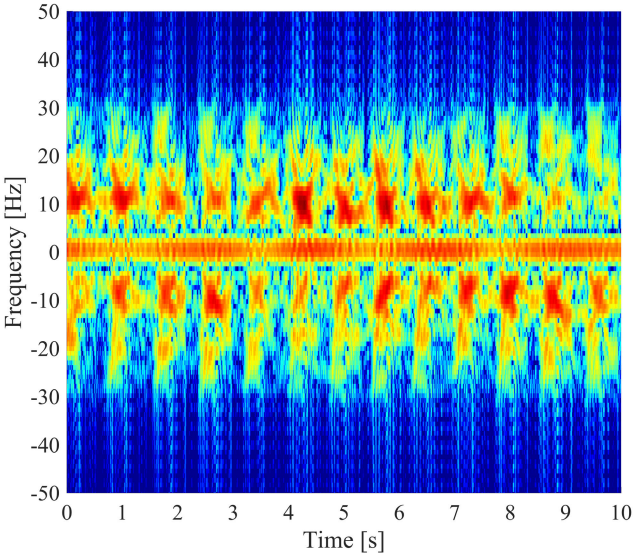

FIGURE 3. An example of a spectrogram obtained from a subject holding his breath.

Many researches have investigated the heartbeat detection via a Doppler sensor to achieve non-contact heartbeat detection without device attachment. Some conventional methods estimate the HR based on frequency analysis by (i) Fast Fourier Transform (FFT) [10], [11], (ii) Wavelet Transform (WT) [12], [13], (iii) Multiple Signal Classification (MUSIC) [14], [15], and DCT [16]. In contrast, by detecting a heartbeat signal over the signal obtained through the extended signal processing, the conventional methods [17]–[23] estimate the BBI. Experimental results have shown that these conventional methods have achieved high HR and BBI estimation accuracies. However, there is no conventional method that can detect the P-wave, the T-wave, and the R-peak, though capturing these features would enable the detection of various diseases. Taking into account that the SNR of the heartbeat components is likely to get degraded due to noise, e.g., respiration and slight body movements, it is more challenging to capture the P-wave, the T-wave, and the R-peak than detecting only heartbeat.

IV. PROPOSED METHOD

In this section, to detect the P-wave, the T-wave, and the R-peak via a Doppler sensor, we propose an ECG signal

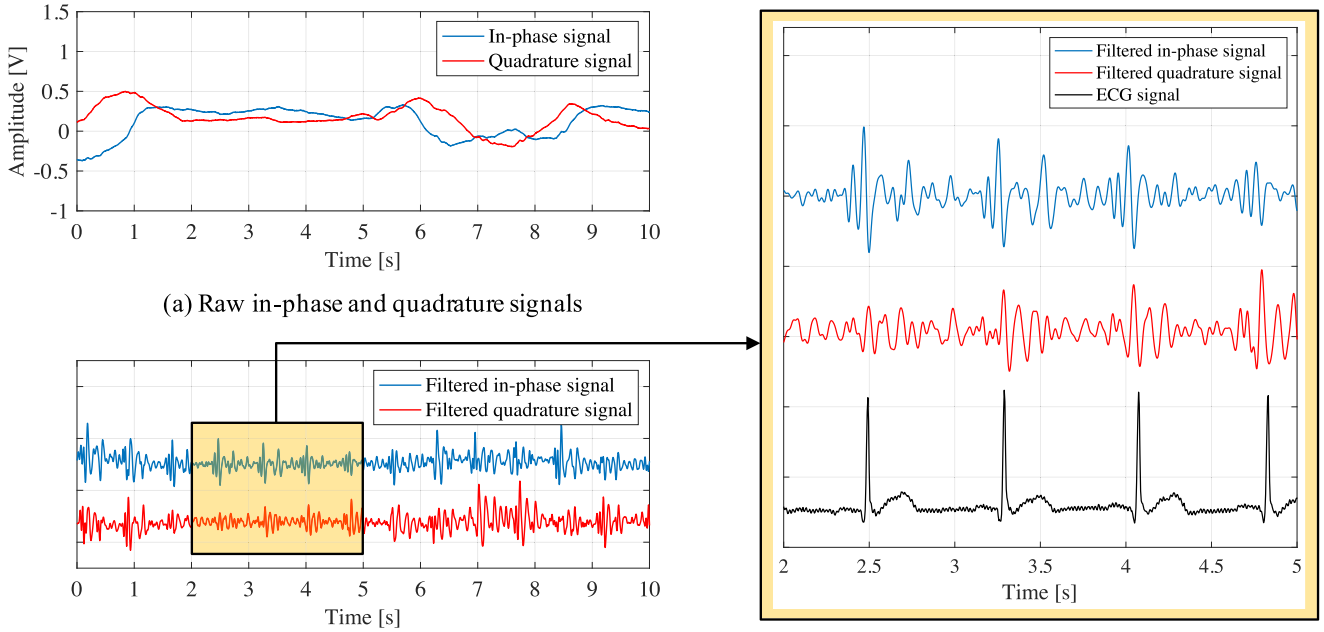

(a) Raw in-phase and quadrature signals

(b) Filtered in-phase and quadrature signals

(c) Zoomed filtered in-phase and quadrature signals

FIGURE 4. Examples of raw in-phase and quadrature signals, and the ones filtered by BPF with the passband of [8.0, 30] Hz.

reconstruction method by a hybrid deep learning model with CNN and LSTM. In what follows, to better understand our proposed method, we first show how heartbeat components appear over a received signal of a Doppler sensor. We then explain the algorithm of the proposed method.

A. HEARTBEAT SIGNAL BY DOPPLER SENSOR

Frequency components due to heartbeats can be divided into two components corresponding to the HR and just one heartbeat. In terms of the HR, the frequency components due to heartbeats typically range from 0.5 Hz to 2.0 Hz, corresponding to 30 beats per minute (bpm) and 120 bpm, respectively. In contrast, the chest's displacement due to heartbeat, x_h, can be expressed as eq. (5) [46].

$$x_h(t) = \nu \cos\{\omega t + \gamma \sin(\Omega t)\}\, e^{-\frac{(t-b)^2}{c}}, \tag{5}$$

where ω and Ω are the parameters used to determine the peak location of a heartbeat signal, and ν and γ are the parameters used to determine the magnitude of the peak. Additionally, b and c are the constant parameters. Based on this model, the previous research [22] has generated the simulated heartbeat signal obtained by a Doppler sensor, and has shown that the frequency components due to the heartbeat signal are distributed in the higher frequency band. Fig. 3 shows an example of a spectrogram obtained from a subject holding his breath. This spectrogram is calculated by Short Time Fourier Transform (STFT) with a 256 ms-time window and a 5 ms-step size. Also, the sampling rate of the Doppler sensor is 1000 Hz, and the number of points in FFT is 1024. From this figure, it can be seen that the spectrum due to each heartbeat appears in the frequency band higher than 2 Hz. Specifically, in our preliminary research [23], we have confirmed that the frequency components due to the heartbeat are mainly distributed from 8.0 Hz to 30 Hz. To associate features of the heartbeat signal with those of the ECG signal, the heartbeat components in such a high frequency band are essential. Fig. 2 shows examples of raw in-phase and quadrature signals and the ones filtered by Band Pass Filter (BPF) with a passband of [8.0, 30] Hz. For a better comparison, an ECG signal is also shown in Fig. 2(c), and the amplitudes of the signals are scaled in Figs. 2(b) and (c). From these figures, we can see the heartbeat signal corresponding to the ECG signal over the filtered in-phase and quadrature signals. However, we can also see that the waveform of the heartbeat signals is not always the same. Thus, in our proposed method, an ECG signal is reconstructed from such a heartbeat signal by relating the features of these two signals to each other based on a deep learning technique.

B. ALGORITHM OF PROPOSED METHOD

In the proposed method, after detecting heartbeat's timing by a heartbeat detection method via the Doppler sensor with a sampling rate of 1000 Hz, a heartbeat signal is segmented by a 1.2 s-time window that is centered at the detected timing. Here, the length of the time window should be set to includes at least one heartbeat, which is very important for reconstructing an ECG signal. In fact, as the heart rate gets lower, the timing when the T-wave appears is likely to be delayed. Based on this fact, we selected a 1.2 s-time window that is long enough to meet this condition. Although a subject who has an ECG

signal longer than 1.2 s may exist, it is possible to change the window length used in our method. More specifically, as aforementioned, the $I(t)$ and the $Q(t)$ filtered by BPF with the passband of [8.0, 30] Hz are segmented as the heartbeat signal. The segmented $I(t)$ and $Q(t)$ are then input to a deep learning model. In the proposed method, an ECG signal is reconstructed by a hybrid model with CNN and LSTM. CNN is a deep learning technique that has the great ability of spatial feature extraction [34]. Typically, CNN has two operations: (i) the convolutional operation and (ii) the pooling operation. Here, let $x^l_{i,j}$ and $w_{p,q}$ denote the elements of the feature map in the layer l and the convolutional filter with the kernel size of $P \times Q$, respectively. With the stride size of the convolutional filter s, the convolutional operation is performed as

$$u_{i,j} = \sum_{p=0}^{P-1} \sum_{q=0}^{Q-1} x_{si+p,sj+q} w_{p,q}. \tag{6}$$

With the activation function of Rectified Linear Units (ReLU), the enhancement of the extracted feature $u_{i,j}$ is performed, and the element of the feature map in the next layer $x^{l+1}_{i,j}$ is obtained as

$$x^{l+1}_{i,j} = \mathrm{ReLU}(u_{i,j}). \tag{7}$$

The pooling operation is performed to reduce the training time by reducing the elements of the feature map, in general. The max pooling algorithm is a typical one used to reduce the size of the feature map, and is used in our proposed model. The max pooling algorithm with the pooling area O in the layer l is performed as

$$x^{l+1}_{i,j} = \max_{(p,q)\in O} x^l_{p,q}. \tag{8}$$

In contrast, LSTM is one of Recurrent Neural Network (RNN) that has been broadly used to analyze time sequence data, and it provides excellent performance of the temporal feature extraction [30]. LSTM typically consists of 4 blocks: (i) the LSTM block, (ii) the input gate, (iii) the forget gate, and (iv) the output gate. Now, let y and h denote input data and hidden states, respectively, and let W, R, p, and b denote the weight from the previous layer, the weight from the hidden layer in the previous time, the peephole weight, and the bias, respectively. The forward-propagation of LSTM is operated as follows.

$$z^{-t} = W_z y^t + R_z h^{t-1} + b_z, \tag{9}$$
$$z^t = \tanh(z^{-t}), \tag{10}$$
$$i^{-t} = W_i y^t + R_i h^{t-1} + p_i \odot c^{t-1} + b_i, \tag{11}$$
$$i^t = \mathrm{sigmoid}(i^{-t}), \tag{12}$$
$$f^{-t} = W_f y^t + R_f h^{t-1} + p_f \odot c^{t-1} + b_f, \tag{13}$$
$$f^t = \mathrm{sigmoid}(f^{-t}), \tag{14}$$
$$c^t = i^t \odot z^t + f^t \odot c^{t-1}, \tag{15}$$
$$o^{-t} = W_o y^t + R_o h^{t-1} + p_o \odot c^{t-1} + b_o, \tag{16}$$
$$o^t = \mathrm{sigmoid}(o^{-t}), \tag{17}$$
$$H^t = o^t \odot \tanh(c^t), \tag{18}$$

where "$\odot$" is the Hadamard product, and the subscripts "z", "i", "f", and "o" denote the LSTM block, the input gate, the forget gate, and the output gate, respectively.

Fig. 5 shows the architecture of the proposed deep learning model. In the proposed method, the segmented $I(t)$ and $Q(t)$ is concatenated, which is an input with the size of 2×800. First, the input is fed into CNN to extract spatial features over the heartbeat signal. This operation makes the model robust against the deformation of the heartbeat signal. Specifically, the convolutional operation by 8 filters with the kernel size of 2×50 is performed, and then the max pooling operation with the kernel size of 1×2 is performed, where the convolutional filter strides by 1 sample, and the pooling area strides without the overlap. Subsequently, the convolutional operation by 8 filters with the kernel size of 2×25 is performed, and then the max pooling operation with the kernel size of 2×2 is performed. Here, the strides of the convolutional filter and the pooling area are the same as mentioned above. To relate the temporal features of the heartbeat signal to those of the

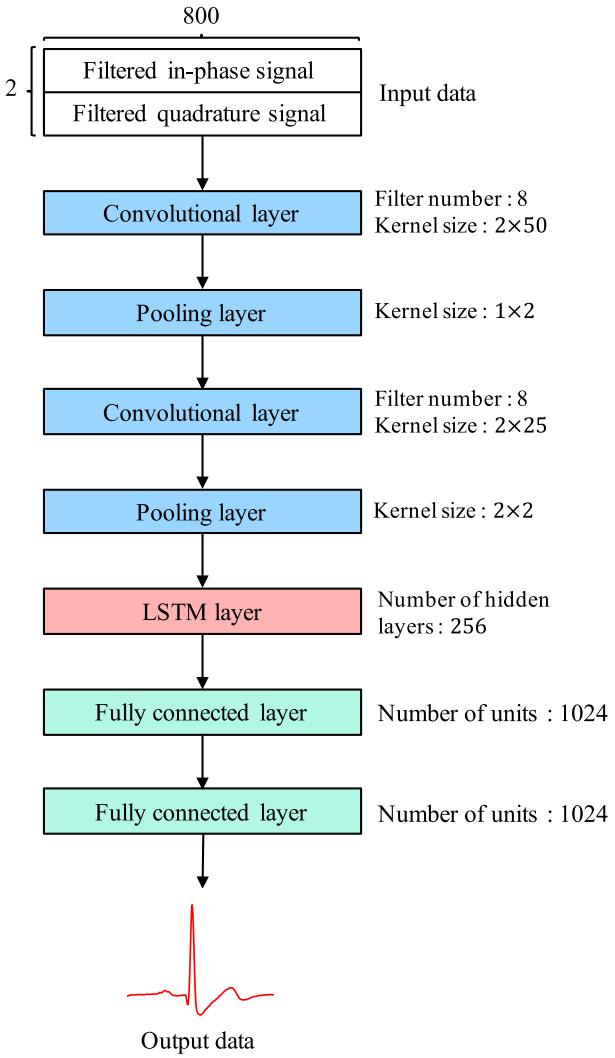

FIGURE 5. The architecture of the proposed deep learning model.

ECG signal, the extracted feature maps are then input to LSTM with 256 hidden layers. Specifically, the output of the CNN can be regarded as the sequence data with a size of 176 × 8 (data length × dimension of features), which is an input to LSTM. Through the fully connected layers with 1024 units, the ECG signal is finally output based on the features obtained by the CNN and LSTM. Here, it is worth mentioning that these parameters used in the model, e.g., the number of filters and the kernel size, should be set considering the over-learning and the reconstruction accuracy of the ECG signal. These can also be adjusted depending on the diversity and the number of training data.

V. EXPERIMENTAL EVALUATION

In this section, we first explain the specification of the experiments and then present the experimental results.

A. EXPERIMENTAL SPECIFICATION

To evaluate the ECG signal reconstruction accuracy of the proposed method, we carried out experiments to collect testing and training data. TABLE 1 lists the experimental specification. We carried out our experiments using a 24 GHz Doppler sensor with the sampling rate of 1000 Hz. We observed heartbeat of 9 subjects for 180 s, and all the subjects were healthy, and do not have abnormalities related with the heart. During the observation, the subjects were lying up on the floor with the natural breathing. The Doppler sensor was attached on the ceiling, and the distance between the Doppler sensor and the subject was 2.5 m. At the same time as the Doppler sensor is used, to collect the actual ECG signal, we observed the subject's heartbeat by an ECG with a sampling rate of 250 Hz. Also, as the loss function to train the proposed model, we used the Mean Squared Error (MSE). The optimizer used to train the model was "Adam", and the number of epochs and the batch size were 40 and 128, respectively.

As the performance metric, we calculated the correlation coefficient κ between the reconstructed and actual ECG signals as

$$\kappa = \frac{\sum_{m=1}^{M}(v_m - \tilde{v})(r_m - \tilde{r})}{\sqrt{\sum_{m=1}^{M}(v_m - \tilde{v})^2}\sqrt{\sum_{m=1}^{M}(r_m - \tilde{r})^2}}, \tag{19}$$

where M denotes the number of samples over the reconstructed and actual ECG signals. v_m and r_m denote the m-th samples over the reconstructed and actual ECG signals, respectively. $\tilde{v}$ and $\tilde{r}$ denote the mean values of the reconstructed and actual ECG signals, respectively. In addition to the correlation coefficient, for the better evaluation of the proposed method, we detected the R-peaks based on the Pan-Tompkins algorithm [47]. This algorithm can detect the R-peak based on an adaptive threshold determined by a signal level. Although it might be possible to detect the R-peak by other algorithm such as the maximum peak detection algorithm, we used the Pan Tompkins algorithm, because it can detect the R-peak accurately, according to previous research related to the SCG-based ECG signal reconstruction [45]. Taking into account that the P peak typically appears within 0.3 s before the R-peak, we thus detected the P peak as the maximum one that appeared within 0.3 s before the R-peak. We finally detected the T peak as the maximum one that appeared after the R-peak. As the performance metric, we calculated the Average Absolute Error (AAE) between the timings when such peaks appeared over the reconstructed and actual ECG signals. Precisely, against each peak, the AAE was calculated as

$$AAE = \frac{1}{N}\sum_{n=1}^{N}|t_{\text{pred}}(n) - t_{\text{true}}(n)|, \tag{20}$$

where N denotes the number of the collected ECG signals, n means the n th ECG signal, and t_{pred} and t_{true} denote the predicted and ground truth timings, respectively. Furthermore, we measured the P-peak to R-peak interval (PRI), R-peak to T-peak interval (RTI), and P-peak to T-peak interval (PTI), and we calculated the Root Mean Squared Error (RMSE) between these intervals over the reconstructed and actual ECG signals as

$$RMSE = \sqrt{\frac{1}{N}\sum_{n=1}^{N}|PPI_{\text{pred}}(n) - PPI_{\text{true}}(n)|^2}, \tag{21}$$

where PPI_{pred} and PPI_{true} denote the peak intervals measured over the reconstructed and actual ECG signals, respectively.

TABLE 1. The specification of the experiment.

Item	Value
Modulation method	Unmodulated continuous wave
Carrier frequency	24 GHz
Sampling frequency	1000 Hz
Number of subjects	9
Observation duration	180 s
Detection range d	2.5 m
Optimizer to train model	Adam
Number of epochs to train model	40
Batch size to train model	128

B. ECG SIGNAL RECONSTRUCTION ACCURACY

TABLE 2 lists the dataset collected through the experiments. In the evaluation of the experiments, we used the hold-out validation to evaluate our proposed method. The data from one set of subjects were used as the testing data, while the other set of subjects were used as the training data, which

TABLE 2. Dataset. *N* denotes the number of the collected heartbeat signals.

ID	Sex	Ave. RRI [ms]	Ave. HR [bpm]	*N*
1	M	886	67.8	192
2	F	887	67.6	184
3	F	818	73.4	192
4	F	837	71.6	188
5	M	1159	51.8	131
6	M	1005	59.7	157
7	M	1043	57.5	144
8	M	1456	41.2	103
9	F	1325	45.3	129

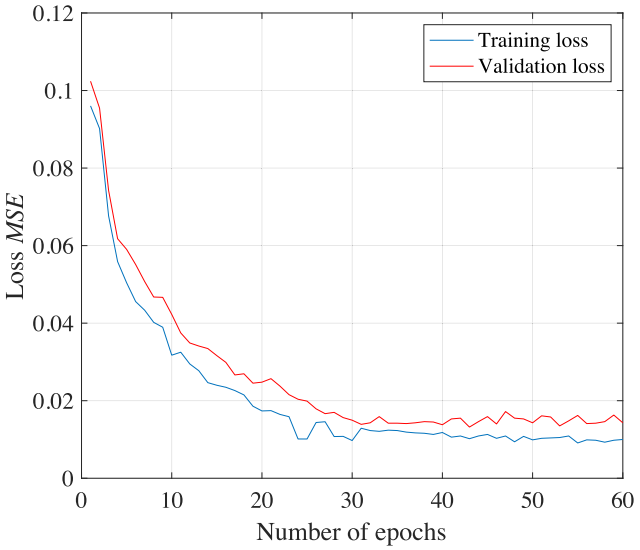

FIGURE 6. The training and validation losses.

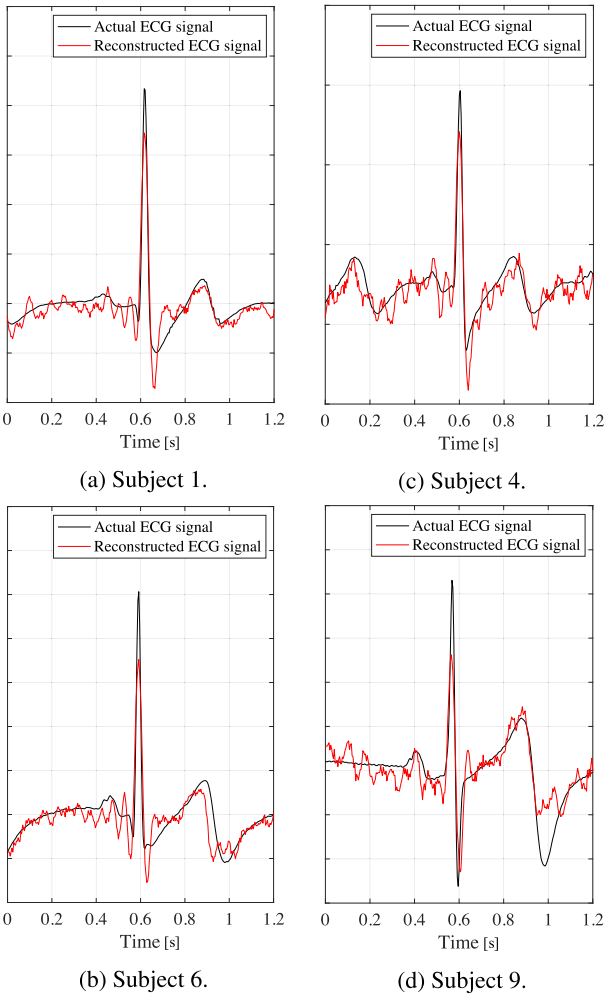

FIGURE 7. Examples of the reconstructed and actual ECG signals.

was repeated for all the subjects. Also, we tried to select the parameters of the deep learning model so that the validation loss was minimized. As for the number of the epochs, we set it based on the convergence of the validation loss. Fig. 6 shows the training and validation losses. From this figure, it can be seen that the validation loss converges at about 0.015 after the epoch 30. In contrast, the training loss decreases slowly even after the epoch 30. In fact, when the training loss continues to decrease in such a way, which leads to the over-learning. Based on this fact, we set the epoch as 40.

Fig. 7 shows examples of the reconstructed and actual ECG signals. In these examples, for a better comparison, the amplitudes of these two signals are scaled. From these examples, it can be seen that the ECG signal is reconstructed by our proposed method so that the P, R and T peaks could be detected. We can also say that detecting the P peak might be difficult, compared to the R and the T peaks. This is because the SNR of the P-wave is low, which makes it challenging to train the proposed deep learning model.

TABLE 3 lists the correlation coefficients κ, the AAEs, and the RMSEs of the proposed method. As seen from this table, our proposed method reconstructs the ECG signal with an average correlation coefficient of 0.86. In general, as the HR gets lower, one period of the ECG signal grows longer, indicating that our method can reconstruct the ECG signal, regardless of the HR. In terms of the AAE, the average AAEs of the P, R, and T peaks are 28.3 ms, 17.8 ms, and 30.3 ms, respectively. From these results, we can say that our method reconstructs R-peak accurately, compared with the P and T ones. The SNRs of the P and T-waves are typically lower than that of the R-peak, and the P and T-wave components over the heartbeat signal by the Doppler sensor are sensitive to noise, e.g., respiration and body movements. Thus, the AAEs of the P and T peaks are lower than that of the R-peak. When a subject has lower HR, the timing when the T-wave appears tends to be delayed. This fact makes it difficult to reconstruct the T-wave, which could be solved by further extending the diversity of the training data. As a result, the RMSEs of

TABLE 3. The correlation coefficients κ, the AAEs, and the RMSEs of the proposed method.

ID	Actual Ave. HR [bpm]	κ	AAE [ms]			RMSE [ms]		
			P	R	T	PRI	RTI	PTI
1	67.8	0.91	30.1	13.6	23.6	29.3	36.3	44.2
2	67.6	0.88	27.3	19.8	24.2	33.5	29.8	39.7
3	73.4	0.89	32.5	22.1	27.4	37.7	35.1	42.5
4	71.6	0.89	23.5	17.8	26.2	28.2	32.8	44.9
5	51.8	0.82	36.7	16.7	38.1	35.9	37.1	54.0
6	59.7	0.85	24.4	14.0	29.5	31.3	34.0	49.5
7	57.5	0.81	29.2	19.1	36.2	27.0	30.4	51.7
8	41.2	0.84	23.3	15.8	34.9	29.5	33.5	46.3
9	45.3	0.83	27.8	21.4	33.0	32.0	36.2	52.2
Ave.	-	0.86	28.3	17.8	30.3	31.6	33.9	47.2

the PRI, RTI, and PTI are 31.6 ms, 33.9 ms, and 47.2 ms, respectively. The required accuracies of the PRI, RTI, and PTI measurements depend on the usage of these intervals. In our future work, we will further improve the ECG signal reconstruction accuracy according to real applications.

C. PERFORMANCE COMPARISON WITH OTHER EXISTING METHODS

TABLE 4 lists the performance comparison of the proposed and the other existing ECG signal reconstruction methods. The three methods in Table 4 use different datasets and sensors, i.e., PPG, SCG, and a Doppler sensor. Thus, the performance comparison among these methods is not necessarily fair. However, to show the ability of the proposed non-contact ECG reconstruction method, it would be beneficial to compare our method with the ones that use the contact sensors. The method [41] reconstructs the ECG signal by the linear transform of the DCT coefficients of the PPG signal to those of the ECG signal. The SCG-based method [45] reconstructs the ECG signal by associating the SCG signal to the ECG signal through bidirectional-LSTM. From this table, it can be seen that the PPG-based ECG signal reconstruction method achieves a high correlation coefficient of 0.96, while our proposed method achieves the correlation coefficient of 0.86. Additionally, the AAEs of the P, R, and T peaks by the SCG-based method are 20 ms, 13 ms, and 16 ms, respectively. In contrast, our method's AAEs for the P, R, and T peaks are 28 ms, 17 ms, and 30 ms, respectively. Although the ECG signal reconstruction accuracy of the conventional methods are higher than that of ours, the experimental results show that our method can reconstruct the ECG signal without the device attachment even in the situation where a subject is 2.5 m away from a Doppler sensor. These results are worth noting, and in our future work, we will try to improve our method to achieve as high an ECG signal reconstruction accuracy as the conventional ones.

TABLE 4. The performance comparison of the proposed and the other existing ECG signal reconstruction methods.

Method	κ	AAE [ms]		
		P	R	T
PPG-based method [41]	0.96	-	-	-
SCG-based method [45]	-	20	13	16
Proposed method	0.86	28	17	30

D. LIMITATION OF PROPOSED METHOD

Our method might not always achieve the good performance of the ECG signal reconstruction, in particular for the types of ECG signal waveforms that are not considered for the training of the model. When a subject has a heart disease that can affect the ECG signal waveform, it is necessary to include such a type of the ECG signal waveform in the training data. Thus, to make our model further robust to the diversity of the ECG signal waveform, numerous training data are essential. Additionally, our method can be applied after the heartbeat detection. When heartbeat is not detected due to noise such as respiration and body movements, it is impossible to reconstruct the ECG signal. Even when the heartbeat is detected, the performance of the ECG signal reconstruction could be degraded due to the large deformation of the heartbeat signal waveform. This issue could also be solved by increasing the diversity of the training data.

VI. CONCLUSION

In this paper, we proposed a Doppler sensor-based Electrocardiogram (ECG) signal reconstruction method by a

hybrid deep learning model with Convolutional Neural Network (CNN) and Long Short-Term Memory (LSTM). As the ECG signal reconstruction method, there exist the ones with the attaching devices, i.e., Photoplethysmography (PPG) and Seismocardiogram (SCG). In contrast, to reconstruct an ECG signal without requiring device attachment, we constructed a deep learning model that outputs the ECG signal by extracting the spatial and the temporal features from a heartbeat signal by a Doppler sensor. Although detecting the P-wave, the T-wave, and the R-peak with a Doppler sensor is more complicated than detecting only heartbeat, because of the low Signal-to-Noise Ratio (SNR) of the heartbeat components, we experimentally confirmed that our proposal performs the ECG signal reconstruction well. In our future work, it is necessary to improve our ECG signal reconstruction accuracy, according to the accuracy required by applications.

REFERENCES

[1] R. E. Kleiger, P. K. Stein, and J. T. Bigger, Jr., "Heart rate variability: Measurement and clinical utility," *Ann. Noninvasive Electrocardiol.*, vol. 10, no. 1, pp. 88–101, Jan. 2005.

[2] J. Allen, "Photoplethysmography and its application in clinical physiological measurement," *Physiol. Meas.*, vol. 28, no. 3, pp. R1–R39, Feb. 2007.

[3] C. Li, V. M. Lubecke, O. Boric-Lubecke, and J. Lin, "A review on recent advances in Doppler radar sensors for noncontact healthcare monitoring," *IEEE Trans. Microw. Theory Techn.*, vol. 61, no. 5, pp. 2046–2060, May 2013.

[4] A. F. Hussein, N. A. Kumar, M. Burbano-Fernandez, G. Ramirez-Gonzalez, E. Abdulhay, and V. H. C. De Albuquerque, "An automated remote cloud-based heart rate variability monitoring system," *IEEE Access*, vol. 6, pp. 77055–77064, 2018.

[5] D. Mocrii, Y. Chen, and P. Musilek, "IoT-based smart homes: A review of system architecture, software, communications, privacy and security," *Internet Things*, vols. 1–2, pp. 81–98, Sep. 2018.

[6] H. Jiang, C. Cai, X. Ma, Y. Yang, and J. Liu, "Smart home based on WiFi sensing: A survey," *IEEE Access*, vol. 6, pp. 13317–13325, 2018.

[7] P. J. Schwartz and M. J. Ackerman, "The long QT syndrome: A transatlantic clinical approach to diagnosis and therapy," *Eur. Heart J.*, vol. 34, no. 40, pp. 3109–3116, Oct. 2013.

[8] P. E. Lazzerini, P. L. Capecchi, and F. Laghi-Pasini, "Long QT syndrome: An emerging role for inflammation and immunity," *Frontiers Cardiovascular Med.*, vol. 2, p. 26, May 2015.

[9] H. Turhan, E. Yetkin, R. Atak, T. Altinok, K. Senen, M. Ileri, and E. Kutuk, "Increased P-wave duration and P-wave dispersion in patients with aortic stenosis," *Ann. Noninvasive Electrocardiol.*, vol. 8, pp. 18–21, Jan. 2003.

[10] G. Vinci, S. Lindner, F. Barbon, S. Mann, M. Hofmann, A. Duda, R. Weigel, and A. Koelpin, "Six-port radar sensor for remote respiration rate and heartbeat vital-sign monitoring," *IEEE Trans. Microw. Theory Techn.*, vol. 61, no. 5, pp. 2093–2100, May 2013.

[11] J. Tu and J. Lin, "Fast acquisition of heart rate in noncontact vital sign radar measurement using Time-Window-Variation technique," *IEEE Trans. Instrum. Meas.*, vol. 65, no. 1, pp. 112–122, Jan. 2016.

[12] M. He, Y. Nian, and B. Liu, "Noncontact heart beat signal extraction based on wavelet transform," in *Proc. 8th Int. Conf. Biomed. Eng. Informat.*, Oct. 2015, pp. 209–213.

[13] M. Li and J. Lin, "Wavelet-Transform-Based Data-Length-Variation technique for fast heart rate detection using 5.8-GHz CW Doppler radar," *IEEE Trans. Microw. Theory Techn.*, vol. 66, no. 1, pp. 568–576, Jan. 2018.

[14] K. J. Lee, C. Park, and B. Lee, "Tracking driver's heart rate by continuous-wave Doppler radar," in *Proc. 38th Annu. Int. Conf. IEEE Eng. Med. Biol. Soc. (EMBC)*, Aug. 2016, pp. 5417–5420.

[15] K. Yamamoto, K. Toyoda, and T. Ohtsuki, "Non-contact heartbeat detection by MUSIC with discrete cosine transform-based parameter adjustment," in *Proc. IEEE Global Commun. Conf. (GLOBECOM)*, Dec. 2018, pp. 1–6.

[16] J. Park, J.-W. Ham, S. Park, D.-H. Kim, S.-J. Park, H. Kang, and S.-O. Park, "Polyphase-basis discrete cosine transform for real-time measurement of heart rate with CW Doppler radar," *IEEE Trans. Microw. Theory Techn.*, vol. 66, no. 3, pp. 1644–1659, Mar. 2018.

[17] C. Will, K. Shi, R. Weigel, and A. Koelpin, "Advanced template matching algorithm for instantaneous heartbeat detection using continuous wave radar systems," in *IEEE MTT-S Int. Microw. Symp. Dig.*, May 2017, pp. 1–4.

[18] I. V. Mikhelson, P. Lee, S. Bakhtiari, T. W. Elmer, A. K. Katsaggelos, and A. V. Sahakian, "Noncontact millimeter-wave real-time detection and tracking of heart rate on an ambulatory subject," *IEEE Trans. Inf. Technol. Biomed.*, vol. 16, no. 5, pp. 927–934, Sep. 2012.

[19] S. Tomii and T. Ohtsuki, "Heartbeat detection by using Doppler radar with wavelet transform based on scale factor learning," in *Proc. IEEE Int. Conf. Commun. (ICC)*, Jun. 2015, pp. 483–488.

[20] T. Sakamoto, R. Imasaka, H. Taki, T. Sato, M. Yoshioka, K. Inoue, T. Fukuda, and H. Sakai, "Feature-based correlation and topological similarity for interbeat interval estimation using ultrawideband radar," *IEEE Trans. Biomed. Eng.*, vol. 63, no. 4, pp. 747–757, Apr. 2016.

[21] W. Hu, Z. Zhao, Y. Wang, H. Zhang, and F. Lin, "Noncontact accurate measurement of cardiopulmonary activity using a compact quadrature Doppler radar sensor," *IEEE Trans. Biomed. Eng.*, vol. 61, no. 3, pp. 725–735, Mar. 2014.

[22] V. L. Petrovic, M. M. Jankovic, A. V. Lupsic, V. R. Mihajlovic, and J. S. Popovic-Bozovic, "High-accuracy real-time monitoring of heart rate variability using 24 GHz continuous-wave Doppler radar," *IEEE Access*, vol. 7, pp. 74721–74733, 2019.

[23] K. Yamamoto, K. Toyoda, and T. Ohtsuki, "Spectrogram-based non-contact RRI estimation by accurate peak detection algorithm," *IEEE Access*, vol. 6, pp. 60369–60379, 2018.

[24] Y. S. Lee, P. N. Pathirana, C. L. Steinfort, and T. Caelli, "Monitoring and analysis of respiratory patterns using microwave Doppler radar," *IEEE J. Transl. Eng. Health Med.*, vol. 2, pp. 1–12, Feb. 2014.

[25] N. T. P. Van, L. Tang, A. Singh, N. D. Minh, and S. C. Mukhopadhyay, "Self-identification respiratory disorder based on continuous wave radar sensor system," *IEEE Access*, vol. 7, pp. 40019–40026, 2019.

[26] H. Zhao, H. Hong, D. Miao, Y. Li, H. Zhang, Y. Zhang, C. Li, and X. Zhu, "A noncontact breathing disorder recognition system using 2.4-GHz digital-IF Doppler radar," *IEEE J. Biomed. Health Informat.*, vol. 23, no. 1, pp. 208–217, Jan. 2019.

[27] B. Y. Su, K. C. Ho, M. J. Rantz, and M. Skubic, "Doppler radar fall activity detection using the wavelet transform," *IEEE Trans. Biomed. Eng.*, vol. 62, no. 3, pp. 865–875, Mar. 2015.

[28] M. G. Amin, Y. D. Zhang, F. Ahmad, and K. C. D. Ho, "Radar signal processing for elderly fall detection: The future for in-home monitoring," *IEEE Signal Process. Mag.*, vol. 33, no. 2, pp. 71–80, Mar. 2016.

[29] S. Z. Gurbuz and M. G. Amin, "Radar-based human-motion recognition with deep learning: Promising applications for indoor monitoring," *IEEE Signal Process. Mag.*, vol. 36, no. 4, pp. 16–28, Jul. 2019.

[30] S. Hochreiter and J. Schmidhuber, "Long short-term memory," *Neural Comput.*, vol. 9, no. 8, pp. 1735–1780, 1997.

[31] Ö. Yildirim, "A novel wavelet sequence based on deep bidirectional LSTM network model for ECG signal classification," *Comput. Biol. Med.*, vol. 96, pp. 189–202, May 2018.

[32] P. Wang, A. Jiang, X. Liu, J. Shang, and L. Zhang, "LSTM-based EEG classification in motor imagery tasks," *IEEE Trans. Neural Syst. Rehabil. Eng.*, vol. 26, no. 11, pp. 2086–2095, Nov. 2018.

[33] R. Wang, X. Liang, X. Zhu, and Y. Xie, "A feasibility of respiration prediction based on deep bi-LSTM for real-time tumor tracking," *IEEE Access*, vol. 6, pp. 51262–51268, 2018.

[34] S. Lawrence, C. L. Giles, A. Chung Tsoi, and A. D. Back, "Face recognition: A convolutional neural-network approach," *IEEE Trans. Neural Netw.*, vol. 8, no. 1, pp. 98–113, Jan. 1997.

[35] O. Ronneberger, P. Fischer, and T. Brox, "U-net: Convolutional networks for biomedical image segmentation," in *Proc. Int. Conf. Med. Image Comput. Comput.-Assist. Intervent.* Cham, Switzerland: Springer, Oct. 2015, pp. 234–241.

[36] K. He, X. Zhang, S. Ren, and J. Sun, "Deep residual learning for image recognition," in *Proc. IEEE Conf. Comput. Vis. Pattern Recognit. (CVPR)*, Jun. 2016, pp. 770–778.

[37] S. Kiranyaz, T. Ince, and M. Gabbouj, "Real-time patient-specific ECG classification by 1-D convolutional neural networks," *IEEE Trans. Biomed. Eng.*, vol. 63, no. 3, pp. 664–675, Mar. 2016.

[38] Z. Zhang, Z. Pi, and B. Liu, "TROIKA: A general framework for heart rate monitoring using wrist-type photoplethysmographic signals during intensive physical exercise," *IEEE Trans. Biomed. Eng.*, vol. 62, no. 2, pp. 522–531, Feb. 2015.
[39] R. W. Wijshoff, M. Mischi, and R. M. Aarts, "Reduction of periodic motion artifacts in photoplethysmography," *IEEE Trans. Biomed. Eng.*, vol. 64, no. 1, pp. 196–207, Jan. 2016.
[40] A. Temko, "Accurate heart rate monitoring during physical exercises using PPG," *IEEE Trans. Biomed. Eng.*, vol. 64, no. 9, pp. 2016–2024, Sep. 2017.
[41] Q. Zhu, X. Tian, C. W. Wong, and M. Wu, "Learning Your Heart Actions From Pulse: ECG Waveform Reconstruction From PPG," *bioRxiv*, Jan. 2019, Art. no. 815258.
[42] M. A. García-González, A. Argelagós-Palau, M. Fernández-Chimeno, and J. Ramos-Castro, "A comparison of heartbeat detectors for the seismocardiogram," in *Proc. IEEE Comput. Cardiol.*, Sep. 2013, pp. 461–464.
[43] Y. Li, X. Tang, and Z. Xu, "An approach of heartbeat segmentation in seismocardiogram by matched-filtering," in *Proc. 7th Int. Conf. Intell. Hum.-Mach. Syst. Cybern.*, vol. 2, Aug. 2015, pp. 47–51.
[44] T. Choudhary, L. N. Sharma, and M. K. Bhuyan, "Standalone heartbeat extraction in SCG signal using variational mode decomposition," in *Proc. Int. Conf. Wireless Commun., Signal Process. Netw. (WiSPNET)*, Mar. 2018, pp. 1–4.
[45] J. Park, H. Cho, W. Hwang, R. K. Balan, and J. Ko, "Deep ECG wave estimation model with seismograph sensor," in *Proc. Int. Mobile Syst., Appl., Services*, Jun. 2019, pp. 568–569.
[46] M. Nosrati and N. Tavassolian, "Accurate Doppler radar-based cardiopulmonary sensing using chest-wall acceleration," *IEEE J. Electromagn., RF Microw. Med. Biol.*, vol. 3, no. 1, pp. 41–47, Mar. 2019.
[47] J. Pan and W. J. Tompkins, "A real-time QRS detection algorithm," *IEEE Trans. Biomed. Eng.*, vol. BME-32, no. 3, pp. 230–236, Mar. 1985.

KOHEI YAMAMOTO (Graduate Student Member, IEEE) was born in Kanagawa, Japan, in 1994. He received the B.E. and M.E. degrees from the Faculty of Science and Technology, Keio University, in 2017 and 2019, respectively, where he is currently pursuing the Ph.D. degree with the Graduate School. His research interest includes signal processing. He is a member of IEICE.

RYOSUKE HIROMATSU (Student Member, IEEE) was born in Tokyo, Japan, in 1995. He received the B.E. and M.E degrees from the Faculty of Science and Technology, Keio University, in 2018 and 2020, respectively.

TOMOAKI OHTSUKI (Senior Member, IEEE) received the B.E., M.E., and Ph.D. degrees in electrical engineering from Keio University, Yokohama, Japan, in 1990, 1992, and 1994, respectively.

From 1994 to 1995, he was a Postdoctoral Fellow and a Visiting Researcher in electrical engineering with Keio University. From 1993 to 1995, he was a Special Researcher of Fellowships of the Japan Society for the Promotion of Science for Japanese Junior Scientists. From 1995 to 2005, he was with the Science University of Tokyo. In 2005, he joined Keio University, where he is currently a Professor. From 1998 to 1999, he was with the Department of Electrical Engineering and Computer Sciences, University of California at Berkeley, Berkeley. He is also involved in research on wireless communications, optical communications, signal processing, and information theory. He has published more than 185 journal articles and 400 international conference papers.

Dr. Ohtsuki is a Fellow of the IEICE and a member of the Engineering Academy of Japan. He was a recipient of the 1997 Inoue Research Award for Young Scientist, the 1997 Hiroshi Ando Memorial Young Engineering Award, the Ericsson Young Scientist Award 2000, the 2002 Funai Information and Science Award for Young Scientist, the IEEE the First Asia-Pacific Young Researcher Award 2001, the Fifth International Communication Foundation (ICF) Research Award, the 2011 IEEE SPCE Outstanding Service Award, the 27th TELECOM System Technology Award, the ETRI Journal's 2012 Best Reviewer Award, and the Ninth International Conference on Communications and Networking in China 2014 (CHINACOM '14) Best Paper Award. He has served as the General Co-Chair and the Symposium Co-Chair of many conferences, including the IEEE GLOBECOM 2008, SPC, the IEEE ICC2011, CTS, the IEEE GCOM2012, SPC, and the IEEE SPAWC. He gave tutorials and keynote speech at many international conferences, including the IEEE VTC and the IEEE PIMRC. He was the Vice President of Communications Society of the IEICE. He is the President of Communications Society of the IEICE. He has served as the Chair of the IEEE Communications Society, Signal Processing for Communications and Electronics Technical Committee. He has also served as a Technical Editor for the *IEEE Wireless Communications Magazine* and an Editor for *Physical Communications* (Elsevier). He is also serving as an Area Editor for the IEEE TRANSACTIONS ON VEHICULAR TECHNOLOGY and an Editor for the IEEE COMMUNICATIONS SURVEYS AND TUTORIALS.